Heat Treat 2021: Proceedings of the 31st ASM Heat Treating Society Conference
September 14–16, 2021
America's Center, St. Louis, Missouri, USA
DOI: 10.31399/asm.cp.ht2021p0125

Effect of Thermomechanical Rolling on the Induction Hardenability of a Micro-alloyed 1045 Steel

Robert Cryderman and Finn Bamrud
Advanced Steel Processing and Products Research Center
Colorado School of Mines
Golden, Colorado, USA
rcryderm@mines.edu

Abstract

A micro-alloyed 1045 steel was commercially rolled into 54 mm diameter bars by conventional hot rolling at 1000 °C and by lower temperature thermomechanical rolling at 800 °C. The lower rolling temperature refined the ferrite-pearlite microstructure and influenced the microstructural response to rapid heating at 200 °C·s^{-1}, a rate that is commonly encountered during single shot induction heating for case hardening. Specimens of both materials were rapidly heated to increasing temperatures in a dilatometer to determine the A_{c1} and A_{c3} transformation temperatures. Microscopy was used to characterize the dissolution of ferrite and cementite. Continuous cooling transformation (CCT) diagrams were developed for rapid austenitizing temperatures 25 °C above the A_{c3} determined by dilatometry. Dilatometry and microstructure evaluation along with hardness tests showed that thermomechanical rolling reduced the austenite grain size and lowered the heating temperature needed to dissolve the ferrite. With complete austenitization at 25 °C above the A_{c3} there was little effect on the CCT behavior.

Introduction

Surface hardening by means of rapid induction heating and quenching has been employed to produce high strength driveline parts for application in automobiles, trucks, and heavy equipment for many years. During induction heating, the surface of the part is rapidly transformed to austenite and quenched to martensite while the core microstructure is unchanged. An example of the thermal cycles involved at different depths during induction hardening a 35 mm diameter shaft is shown in Fig. 1 [1]. Near the surface, the induction heating temperature is high enough to exceed the A_{c3} temperature where full transformation to austenite occurs. At deeper depths in the transition zone, the steel is heated to temperatures between the A_{c1} and A_{c3} temperatures where partial transformation to austenite takes place. At still deeper depths, there is no transformation to austenite, but the core microstructure is rapidly sub-critical annealed.

Engineers are driven by the need to design lighter parts and by the desire for higher strength components to withstand the higher torques from higher powered internal combustion engines or advanced battery electric vehicles. It has been shown that modifying the induction heating cycles at the surface to use lower austenitizing temperatures for shorter times can refine the austenite grain size, leading to increases in the torsional fatigue strength and notched fracture resistance [2,3].

The microstructure of a component prior to induction hardening has a major effect on the energy, temperature, and time needed for austenitizing. Tests on SAE 1541 and 5150 steels have shown that the prior microstructure has a strong effect on the depth of hardening for a fixed induction hardening cycle [4,5]. As shown in Fig. 2 the depth of hardening increased for a 1541 steel in order from the shallowest for a spheroidized carbide microstructure, to coarse ferrite-pearlite, to pearlite-bainite, to the deepest for an initial martensitic microstructure [4]. A similar study using 1550 and 5150 steels showed that the depths of hardening for furnace cooled coarse ferrite-pearlite microstructures (referred to as lamellar pearlite annealing) were substantially shallower than those for water quenched martensite at short, 0.75 s, induction heating times [5]. This change in behavior is the result of the kinetics of dissolution of the ferrite and carbide micro-constituents in austenite as affected by both the temperature and the time at temperature.

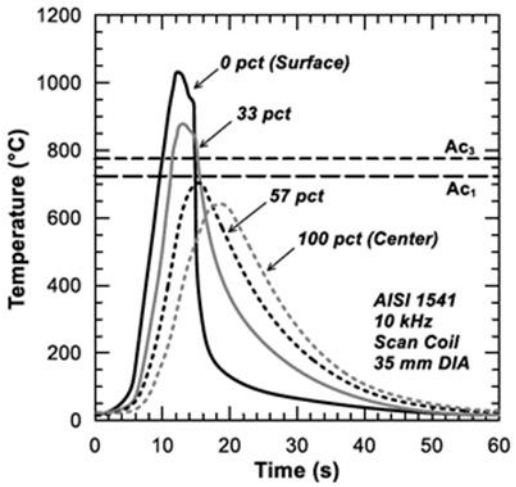

Figure 1: Thermal cycles calculated by electro-thermal modeling for induction heating a 35 mm diameter shaft [1].

Also, it has been shown that increased heating rates increased both the A_{c1} and the A_{c3} temperatures for both carbon and low alloy steels [6-8], thus requiring higher austenitizing temperatures for full transformation to austenite before quenching.

In industry, both as hot rolled (HR) ferrite-pearlite microstructures and quenched and tempered microstructures are employed to produce high strength induction hardened shafts, typically for drive axles and steering racks, used in

automotive and truck applications. Quenching and tempering prior to induction hardening provides a benefit for fatigue strength due to the higher core hardness, but has the disadvantage of higher cost. Typical HR ferrite-pearlite steel exhibits less than optimum induction hardenability due to the scale of the ferrite and pearlite micro-constituents and the resulting kinetics of ferrite and pearlite dissolution.

It has been shown that by thermomechanical rolling (TMR) it is possible to refine and elongate the austenite grains and, consequently, produce a ferrite-pearlite microstructure with smaller ferrite grains and pearlite nodules [9]. The purpose of this study is to examine the effects of the finer TMR microstructure on induction hardenability.

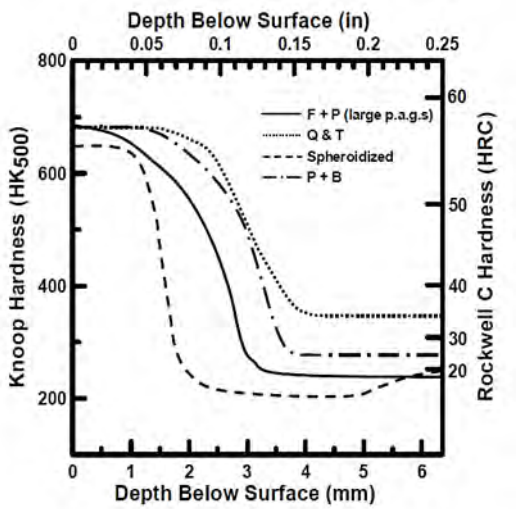

Figure 2: Effects of prior microstructure in 1541 steel on the hardness profiles after induction hardening to constant thermal schedules [4].

Experimental Materials

One commercially produced heat of 10V45Nb steel with the chemical composition shown in Table 1 was used in this investigation.

Table 1: Chemical Composition of 10V45Nb Test Steel (wt pct)

C	Mn	P	S	Si	Cr	Ni
0.46	0.85	0.01	0.03	0.27	0.14	0.08

Mo	Cu	Al	Nb	V	N
0.03	0.16	0.00	0.020	0.092	0.0124

This heat was micro-alloyed with vanadium to increase the as-rolled core strength and with niobium to restrict austenite grain recrystallization during low temperature rolling [10,11]. One part of the heat was HR with a finish rolling temperature of 1000 ºC. Another part was TMR at a finish rolling temperature of 800 ºC that was achieved by cooling the bar after the rough rolling passes and before the finish rolling passes. Both materials were finish rolled into 54 mm diameter bars. Additional details of the rolling processes have been described previously [9].

The light optical microstructures (LOM) for these two rolling processes are shown in Fig. 3. An examination of the LOM for the 10V45Nb HR in Figs. 3(a) and 3(b) shows that there was little difference in the grain structure when viewing the longitudinal and transverse sections. Comparison of the LOM for the 10V45Nb TMR in Figs. 3(c) and 3(d) shows that the ferrite and pearlite areas were clearly elongated in the direction parallel to the rolling direction. This elongated appearance is the result of rolling the austenite at a temperature below the recrystallization temperature. The elongated austenite grains then transformed to ferrite and pearlite with ferrite predominantly nucleating on the deformed austenite grain boundaries followed by transformation of the remaining austenite to pearlite. The area fraction of ferrite was previously determined to be higher after TMR at 64 pct as compared to 44 pct after HR [9]. Also, the ferrite grain size measured on the transverse plane was determined to be smaller for the TMR bar at 7.1 μm as compared to 10.3 μm for the HR bar [12]. Comparison of the LOM in Fig. 3 also shows that the pearlite nodule size and the distance between ferrite areas is much smaller for the TMR bar than for the HR bar.

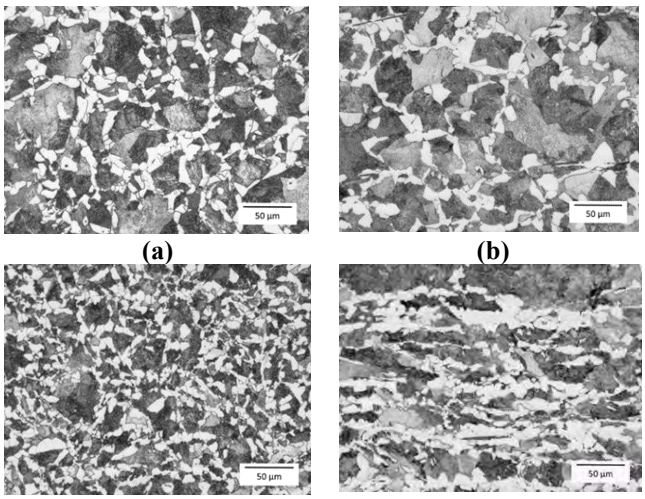

Figure 3: Light optical microstructures of as-rolled bars after etching with 2 pct nital (a), (b) HR, (c), (d) TMR, (a), (c) transverse plane and (b), (d) longitudinal plane.

Dilatometry

A TA 805L dilatometer was used for simulating induction heating and evaluating hardenability. This unit consists of an induction coil for heating, a gas quench unit for cooling, and a linear voltage displacement transducer (LVDT) connected to the ends of the specimen by 4 mm diameter fused silica tubes to measure changes in length. The specimens, 4 mm diameter by 10 mm long, were machined such that the specimen center axis was parallel to the rolling direction at a distance of 4 mm from the bar surface. Accordingly, the entire specimen was located at least 2 mm below the bar surface. A thermocouple was welded to the surface at the center of the specimen for temperature control and recording. A programmed heating rate of 200 $^{o}C \cdot s^{-1}$ was used for all tests, as this is the maximum heating rate that the induction heating system could attain in austenite for the 4 mm diameter solid specimens.

Typical heating and induction power demand curves are shown in Fig. 4(a) as a function of time. The slope of the heating curve

was constant up to the beginning of transformation to austenite, at which point the induction power increased to the maximum 100 pct. There was a deviation in the slope during transformation to austenite and then a return to the programmed slope for heating the austenite at 100 pct power. The corresponding dilation plot during heating is shown in Fig. 4(b). It should be noted that there was an unexpected anomalous expansion at the A_{c1} temperature which is a result of non-uniform heating at the specimen ends. Tests have shown that during heating at 200 $^{o}C \cdot s^{-1}$ the specimen ends are approximately 50 ^{o}C colder than the specimen center and the ends continue to heat at this rate while the center transforms to austenite and heats at a much lower rate resulting in the anomalous expansion [13,14]. For this study, the A_{c1} temperature was defined as the temperature at which the slope of the dilation plot became negative, i.e. at the peak in the curve shown in Fig. 4(b).

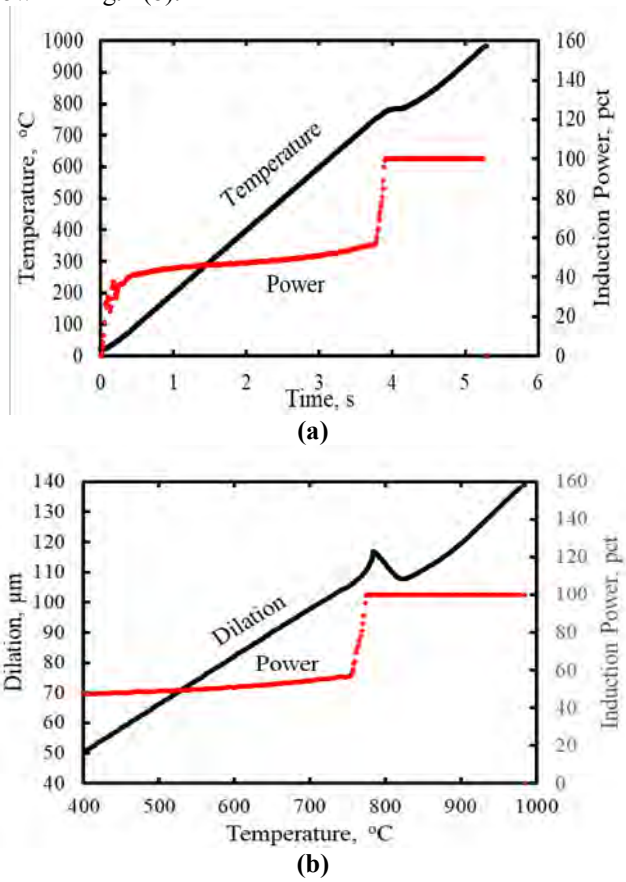

Figure 4: Typical dilatometric data during heating a 10V45Nb HR specimen at 200 $^{o}C \cdot s^{-1}$ (a) temperature and power versus time and (b) dilation and power versus temperature.

Hardness Tests and Metallography

For all test conditions, circular cross sections were cut from the mid-point of the 10 mm long dilatometer specimens where the center thermocouple was located. This sectioning presented the transverse plane relative to the original rolling direction for subsequent metallographic and hardness testing. The specimens were mounted in bakelite and polished through 1 µm diamond suspension. Hardness tests were conducted using an automated tester with a 500 g load. Twenty-five tests were conducted on each circular cross section, and the average of the 25 tests are reported. The cross-sectional specimens utilized for the hardness tests were polished through 1 µm diamond suspension, etched with 2 vol pct nital and examined by light optical microscopy (LOM). Scanning electron microscopy (SEM) was also performed on some of the nital etched specimens.

Effects of Peak Heating Temperature

Specimens of each material were heated to selected peak temperatures at 200 $^{o}C \cdot s^{-1}$ and helium quenched at the rate of 235 $^{o}C \cdot s^{-1}$. Dilation data were analyzed to determine the A_{c1} and A_{c3} temperatures and LOM microstructures were evaluated to determine the temperature needed to fully dissolve the pro-eutectoid ferrite. Dilation data for individual tests of the 10V45Nb HR and 10V45Nb TMR materials are shown in Fig. 5. The data for specimens heated to a peak temperature above 970 ^{o}C indicate that the A_{c3} temperature for the 10V45Nb TMR steel at 888 ^{o}C was about 32 ^{o}C lower than the A_{c3} temperature of 920 ^{o}C for the 10V45Nb HR steel. Similarly, the A_{c1} temperature for the 10V45Nb TMR specimen was 14 ^{o}C lower than the A_{c1} temperature for the 10V45Nb HR specimen.

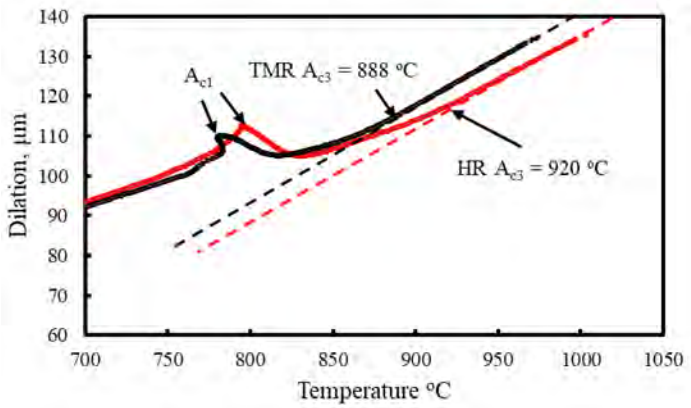

Figure 5: Comparison of dilation for single tests of steel 10V45Nb HR and steel 10V45Nb TMR during heating at 200 $^{o}C \cdot s^{-1}$ showing A_{c3} temperatures of 920 ^{o}C and 888 ^{o}C, respectively.

During the course of dilatometry testing, specimens were heated to a series of increasing temperatures and immediately helium quenched to assess the progress of transformation to austenite. The average values of the A_{c1}, A_{c3}, and M_s temperatures were determined by testing several specimens heated to temperatures more than 40 ^{o}C above the A_{c3} temperatures. The average values and the number of tests for each material are listed in Table 2. M_s temperatures were determined by dilatometry during helium quenching and these values, as given in Table 2, indicate a 12 ^{o}C lower M_s temperature for the TMR condition.

Table 2: Average Transformation Temperatures, ^{o}C, for Test Steels During Heating at 200 $^{o}C \cdot s^{-1}$ and During Quenching at 235 $^{o}C \cdot s^{-1}$.

Steel	Tests	A_{c1}	A_{c3}	M_s
10V45Nb TMR	3	781	895	339
10V45Nb HR	4	787	904	351

Martensitic microstructures of the 10V45Nb steels evaluated by LOM after heating to the indicated peak temperatures and helium quenching are shown in Fig. 6. For austenitizing temperatures below the A_{c3}, undissolved proeutectoid ferrite can be readily seen in Figs. 6(a) and 6(b). For austenitizing temperatures above the A_{c3} temperatures as shown in Figs. 6(c) and 6(d), there is no evidence of undissolved ferrite, but there are darker etching regions at the former ferrite regions that are likely to be bainite or low carbon martensite that formed during helium quenching. It should be noted that the spacing and size of the remaining proeutectoid ferrite grains below the A_{c3} is smaller for the TMR (Fig. 6(b)) as compared to the HR (Fig. 6(a)) condition. Specimens from Figs. 6(c) and 6(d) were examined by SEM and are shown in Fig. 7. At low magnification in Figs. 7(a) and 7(b), the lighter patterns are similar to those shown as darker etching patterns in Figs. 6(c) and 6(d), respectively, and the lighter contrast areas are less evident for the TMR specimen. Closer examination of these lighter regions as shown in Figs. 7(c), 7(d), 7(e), and 7(f) show that they are predominantly bainite or low carbon martensite. These lighter contrast regions are considerably smaller for the TMR (Figs. 7(d) and 7(f)) as compared to the HR (Figs. 7(c)) and 7(e)) and correlate with the appearance at the lower magnification (Figs. 7(a) and 7(b)).

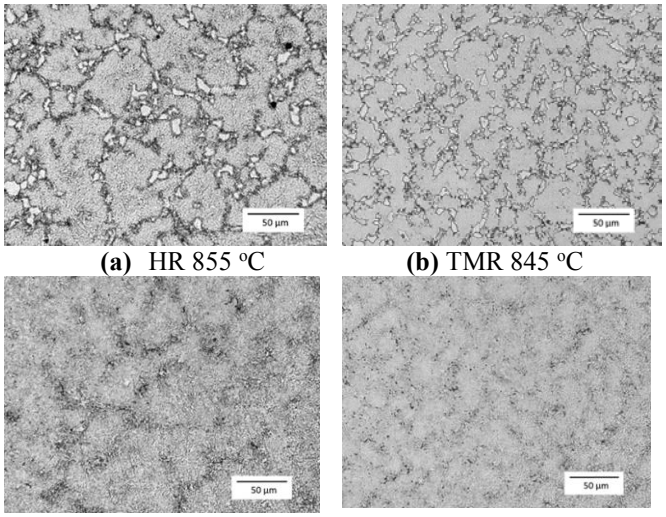

(a) HR 855 °C **(b)** TMR 845 °C

(c) HR 952 °C **(d)** TMR 944 °C

Figure 6: LOM Microstructures of (a, c) steel 10V45Nb HR and (b, d) steel 10V45Nb TMR after heating at 200 °C·s^{-1} to temperatures below (a, b) and above (c, d) the A_{c3} temperatures determined from dilatometry.

It is likely that these bainitic regions at the former ferrite locations were lower in carbon content due to limited time for carbon diffusion after transformation to austenite. The pro-eutectoid ferrite shown in Figs. 6(a) and 6(b) originally formed at the austenite grain boundaries from HR or TMR, and these former pro-eutectoid ferrite regions were predominantly located at austenite grain boundaries that formed during the simulated induction heating cycle. Consequently, the finer initial TMR microstructure (Fig. 3(c) versus Fig. 3(a)) carried through to the simulated induction heated austenite microstructure indicating a smaller austenite grain size for TMR as compared to HR.

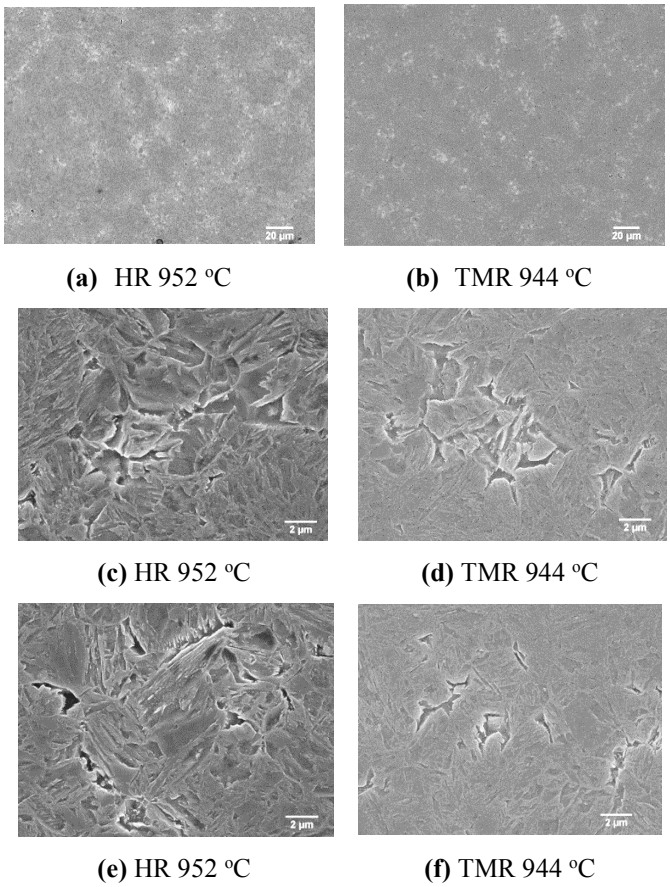

(a) HR 952 °C **(b)** TMR 944 °C

(c) HR 952 °C **(d)** TMR 944 °C

(e) HR 952 °C **(f)** TMR 944 °C

Figure 7: SEM microstructures of (a), (c), (e) steel 10V45Nb HR and (b), (d), (f) steel 10V45Nb TMR after heating at 200 °C·s^{-1} to 48 °C above the respective A_{c3} temperatures.

Hardness test results for the peak temperature heating series are summarized in Fig. 8. As expected, the hardness values reached the highest levels by heating above the A_{c3} temperatures. The plots in Fig. 8 indicate that the hardness was higher at a given peak heating temperature for the 1045TMR steel as compared to the 1045HR steel up to about 975 °C, well above the A_{c3} temperature for both steels.

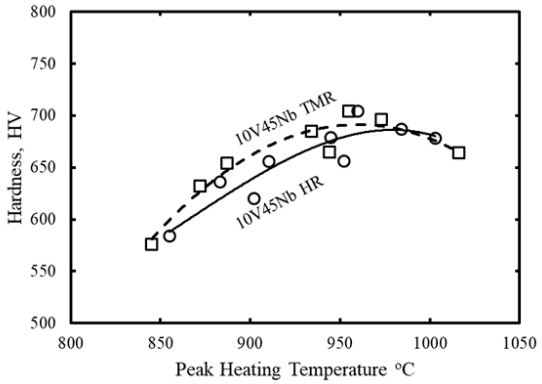

Figure 8: Effects of rapid 200 °C·s^{-1} peak heating temperature on the hardness of the test steels 10V45Nb HR and 10V45Nb TMR.

The increasing hardness values after heating to progressively higher temperatures above the A_{c3} temperatures, suggest that cementite dissolution and carbon diffusion continued at

temperatures above the A_{c3} temperature determined from dilatometry.

Effects of Cooling Rate

A series of tests were conducted with the 10V45Nb HR and 10V45Nb TMR steels using rapid heating at 200 $^{o}C \cdot s^{-1}$ to a temperature approximately 25 ^{o}C above the A_{c3} temperature followed by immediate cooling at different rates to develop continuous cooling transformation (CCT) diagrams.

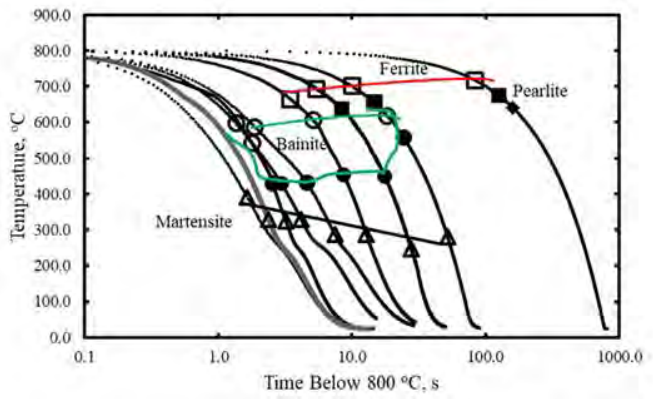

(a)

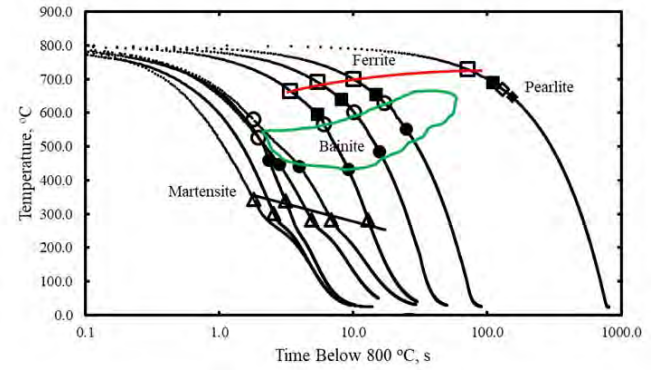

(b)

Figure 9: CCT diagrams for (a)10V45Nb HR steel and (b) 10V45Nb TMR steel after heating at 200 $^{o}C \cdot s^{-1}$ to 925 ± 10 ^{o}C and cooling at selected rates.

The CCT diagrams for the 10V45Nb HR and 10V45Nb TMR steels are shown in Figs. 9(a) and 9(b), respectively. Cooling rates of 235, 200, 150, 73, 40, 20, 10, and 1 $^{o}C \cdot s^{-1}$ over the range of 800 to 300 ^{o}C were used to develop the CCT diagrams. Corresponding LOM micrographs for selected cooling rates are shown in Fig. 10. The general appearance of the CCT diagrams is similar for the two 10V45Nb steel conditions with only martensite detected for the two fastest cooling rates. Cooling at 150 $^{o}C \cdot s^{-1}$ resulted in the formation of small amounts of bainite in a martensitic matrix detected by dilatometry and shown in Figs. 10(a) and 10(b). An increased amount of bainite formed when cooling at 76 $^{o}C \cdot s^{-1}$ as detected by dilatometry and confirmed by LOM as shown in Figs. 10(c) and 10(d). With cooling at 10 $^{o}C \cdot s^{-1}$, ferrite is formed followed by pearlite and/or bainite as shown in Figs. 10(e) and 10(f). Cooling at 1 $^{o}C \cdot s^{-1}$ produced ferrite and pearlite. The temperatures for the start of transformation to martensite (M_s) decreased with reduced cooling rates due to increased carbon content in the austenite as the transformations to bainite and/or ferrite rejected carbon to the remaining austenite and the M_s dropped in accordance with the well-established correlation between M_s and carbon content [15].

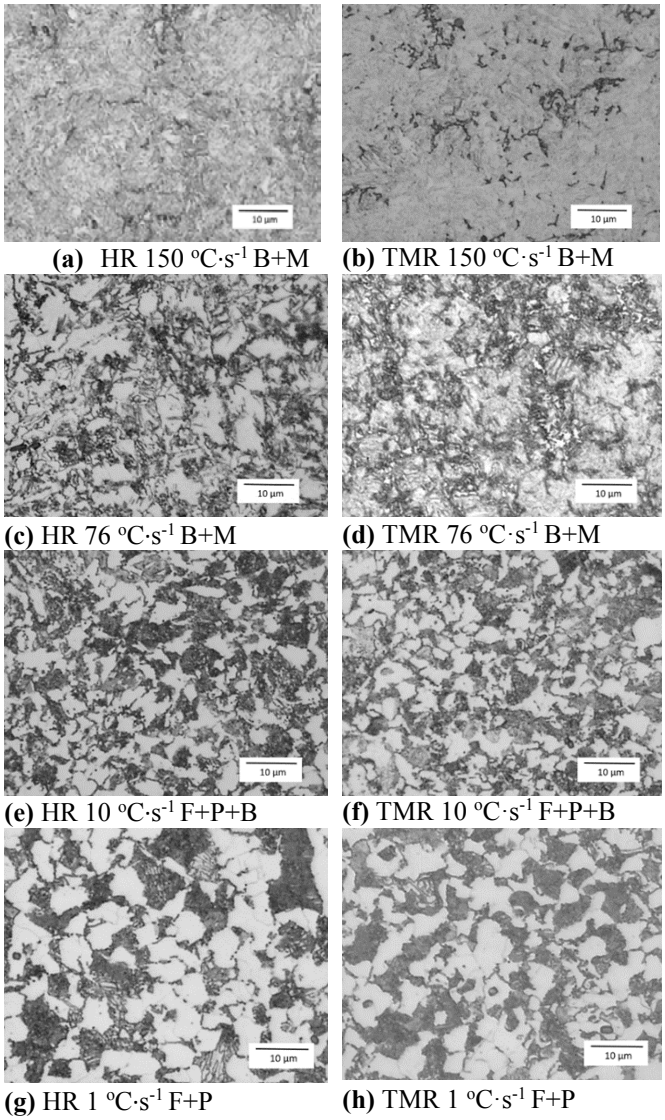

(a) HR 150 $^{o}C \cdot s^{-1}$ B+M **(b)** TMR 150 $^{o}C \cdot s^{-1}$ B+M

(c) HR 76 $^{o}C \cdot s^{-1}$ B+M **(d)** TMR 76 $^{o}C \cdot s^{-1}$ B+M

(e) HR 10 $^{o}C \cdot s^{-1}$ F+P+B **(f)** TMR 10 $^{o}C \cdot s^{-1}$ F+P+B

(g) HR 1 $^{o}C \cdot s^{-1}$ F+P **(h)** TMR 1 $^{o}C \cdot s^{-1}$ F+P

Figure 10: LOM microstructures of 10V45Nb HR (a), (c), (e), (g) and 10V45Nb TMR (b), (d), (f), and (h) specimens cooled at indicated rates and etched in 2 vol pct nital. M=martensite, B= bainite, F= ferrite, and P=pearlite.

Hardness tests were conducted on specimens for each cooling rate. The test results for the 10V45Nb steel in both rolling conditions are compared in Fig. 11 where the fitted curves are virtually identical. The hardness results confirm the observation from the CCT diagrams that there is no appreciable difference in the transformation behavior between the 10V45Nb TMR and 10V45Nb HR materials when the austenitizing temperature was 25 ^{o}C above the A_{c3} temperature.

It could be anticipated that the smaller austenite grain size for the TMR steel would transform more quickly to non-martensitic transformation products during cooling. However, the increase in the dissolution rate during heating for the TMR

steel appears to increase the hardenability enough to offset the reduction in hardenability from the smaller austenite grain size.

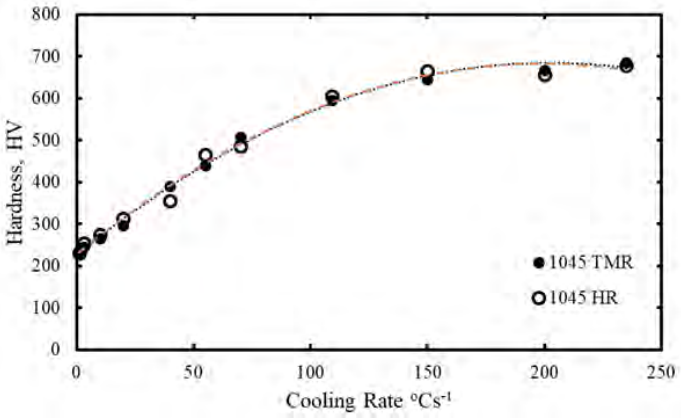

Figure 11: Hardness of test specimens heat treated according to the cooling rates used to develop the CCT diagram.

Summary and Conclusions

Two billets from one commercial heat of micro-alloyed 10V45Nb steel containing 0.09 wt pct V and0.02 wt pct Nb were rolled into 54 mm diameter bars; one using normal the normal HR process with a finish rolling temperature of 1,000 °C and one using a TMR process with a finish rolling temperature of 800 °C. The TMR bar had a finer ferrite-pearlite microstructure and smaller pearlite nodule size than the ferrite-pearlite microstructure in the HR bar (Fig. 3).

The finer structure of the 10V45Nb TMR steel as compared to the HR condition provided a benefit in lowering the A_{c1} and A_{c3} temperatures (Table 2) and increasing the hardness at low austenitizing temperatures (Fig. 8). The initial TMR condition also resulted in a smaller austenite grain size during rapid heating and quenching (Fig. 6).

The CCT diagrams after rapid heating to 25 °C above the A_{c3} temperatures were similar for the 10V45Nb TMR and HR steels with a critical cooling rate of 200 $°C \cdot s^{-1}$ to attain 100 pct martensite (Figs. 9 and 10). This behavior was confirmed by hardness data (Fig. 11). Overall, it is apparent that the TMR improves the ease of austenitizing during rapid heating but does not appreciably change the transformation kinetics during cooling for a fixed austenitizing temperature. Lowering the austenitizing temperature may alter the CCT behavior.

The data obtained at a heating rate of 200 $°C \cdot s^{-1}$ is adequate for simulating single shot hardening but may not accurately reflect the behavior at scanning induction heating rates of 1000 $°C \cdot s^{-1}$. An investigation is underway to increase the maximum heating rate on the dilatometer by modifying the test specimen dimensions.

Acknowledgements

The authors acknowledge the support of the corporate sponsors of the Advanced Steel Processing and Products Research Center, an industry/university cooperative research center at the Colorado School of Mines. Special thanks to Gerdau Special Steels North America for supplying the test materials.

References

1. Z. Li, B. L. Ferguson, V. Nemkov, R. Goldstein, J. Jackowski, and G. Fett, "Effect of Quenching Rate on Distortion and Residual Stresses During Induction Hardening of a Full-Float Truck Axle Shaft," *Journal of Materials Engineering and Performance,* vol. 23, no. 12, pp. 4170-4180, 2014.
2. K. Fukuzawa, Y. Misaka, and K. Kawasaki, "The Effects of Grain Refinement on the Fatigue Properties of Induction Hardened Cr-Mo Steel," *Proceedings. 17th IFHTSE Congress,* Kobe, Japan, Oct 27-30, 2008.
3. R. L. Cryderman and J.G. Speer, "Microstructure and Notched Fracture Resistance of 0.56% C Steels After Simulated Induction Hardening," *Heat Treat 2017: Proceedings of the 29th ASM Heat Treating Society Conference,* October 24–26, 2017, Columbus, Ohio, USA
4. J. Coryell, D. Matlock, and J. Speer, "The Effect of Induction Hardening on the Mechanical Properties of Steel with Controlled Prior Microstructures," *Heat Treating for the 21 st Century: Vision 2020 and New Materials Development, Proceedings of Materials Science and Technology,* AIST, Warrendale, PA, 2005, pp. 3-14.
5. D. Medlin, G. Krauss, and S. Thompson, "Induction Hardening Response of 1550 and 5150 Steels with Similar Prior Microstructures," *Proceedings of First International Conference on Induction Hardening of Gears and Critical Components,* Gear Research Institute. Evanston, Il, pp. 57-66, 1995.
6. S. Semiatin and D. Stutz, *Induction Heat Treatment of Steel*, ASM International, 1986.
7. J. Orlich, A. Rose, and P. Wiest, Ed., "*Atlas zur Warmbehandlung der Staehle, Vol 3*, Zeit-Temperatur-Austenitisierung-Schaubilder", Verlag Stahleisen mbH Duesseldorf Germany, 1973.
8. R. Cryderman, D. Garrett, Z. Schlittenhart, and E. Seo, "Effects of Rapid Induction Heating on Transformations in 0.6% C Steels," *Journal of Materials Engineering and Performance*, ASM, Feb 2020, doi.org/10.1007/s11665-020-04632-0
9. B. Whitley, C. Easter, R. Cryderman, J. Speer**,** **"**Thermomechanical Simulation and Microstructural Analysis of Microalloyed Medium Carbon Bar Steels," *Conference Proceedings of Long and Forged Products*, Vail, Colorado, AIST, July 2015
10. G. Krauss, Steels – *Processing, Structure, and Performance, 2nd edition*, ASM International. pp. 303-304, 2015.
11. S. Vervynckt, K. Verbeken, P. Thibaux, M. Liebeherr, and Y. Houbaert, "Austenite Recrystallization–Precipitation Interaction in Niobium Microalloyed Steels," *ISIJ International, Volume 49, Issue 6* pp. 911-920, 2009.
12. B. Whitley, "Thermomechanical Processing Of Microalloyed Bar Steels For Induction Hardened Components," PhD Thesis, Colorado School of Mines, 2015.

13. R. Goldstein, T. Eddir, E. Buchner, R. Cryderman, A. Banka, and A. Senita, "Modeling of Temperature Gradients During Short Time Dilatometry Testing," *Journal of Materials Engineering and Performance*, ASM International, 2020, doi.org/10.1007/s11665-020-04862-2.
14. G. Krauss, Steels – Processing, Structure, and Performance, 2nd edition, ASM International. p. 80, 2015